RADAR BACK-SCATTER FROM THE SEA SURFACE

K. Hasselmann* and M. Schieler
Institut fuer Geophysik
University of Hamburg

ABSTRACT

Doppler spectra of electromagnetic backscatter from the sea surface are interpreted in terms of generalized Bragg models. The observed broadening of the spectra about the Bragg line is attributed to higher-order nonlinear processes. At conventional radar frequencies, good agreement with the measurements is achieved by an extension of the wave-facet interaction model considered by Wright, Bass et al. and other workers. The correlation of wave slopes and orbital velocities in the joint probability distribution of carrier-wave facets leads to significant differences between the Doppler spectra for vertical, horizontal and cross polarization. In the HF band, the Doppler broadening is interpreted in terms of quadratic wave-wave interactions. For the usual case that the electromagnetic wave lengths are small compared with the principal wave lengths of the sea, the theoretical Doppler spectrum consists of the lowest-order Bragg line and superimposed images of the complete ocean wave frequency spectrum folded on either side of the Bragg line. Both wave-facet and wave-wave interaction models give promise of extracting significant information on the "state of the sea" from electromagnetic Doppler return at wave lengths short compared with the dominant wave lengths of the sea.

*Presently at Woods Oceanographic Institution.

I. INTRODUCTION

The development of numerical wave prediction methods in the past years [1, 2, 17] has increased the need for wave data on a synoptic scale, both as a reference for testing and improving the models and as real-time input for the computations. Synoptic wave data would also be of value for numerical weather forecasting by providing indirect information on surface winds in otherwise poorly covered areas of the oceans. The growing interest in electromagnetic backscatter from the sea surface stems largely from the potentiality of the method for furnishing sea-state data of this kind. Radar scatterometers in satellites could scan most of the world oceans in a few hours. Alternatively, large areas of the ocean can be sampled using HF stations on land. Following the pioneering work of Crombie [6] and others, Ward [22] has recently detected the backscattered return of ionospheric HF modes from relatively small, 100 km square patches of the sea surface at distances up to 3000 km.

Unfortunately, both techniques suffer from wave length limitations. Cloud absorption and finite atenna size define an effective transmission window for satellite scatterometers in the conventional radar wave length range between a few fractions of a cm and about 50 cms. Backscatter measurements over long horizontal ranges are similarly restricted to ionospheric modes in the decameter band. In both cases, the electromagnetic wave lengths are considerably shorter than the principal components of the surface-wave spectrum, which normally lie in the range between 50 and 500 m. The bad wave length matching creates difficulties in relating the backscattered signals obtained by these methods to significant sea-state parameters.

Scattering experiments in both the centimeter-decimeter and decameter bands have now clearly established the basic validity of the first-order (Bragg) wave-wave interaction theory. According to this model, the backscattered radiation arises from interactions with two gravity-wave components whose wavenumbers $\underset{\sim}{k}^g$ are determined by the Bragg (resonance interaction) condition for constructive interference, $\underset{\sim}{k}^g = \pm 2\underset{\sim}{k}^i$, where $\underset{\sim}{k}^i$ represents the horizontal wavenumber component of the incident radiation. For non-normal incidence, the wave lengths of the scattering and incident components are then of the same order, which implies that the scattering surface waves normally lie in the high-wavenumber, equilibrium range of the surface-wave spectrum. It appears therefore from first-order theory that backscatter measurements may yield a useful independent determination of Phillips' constant [15, 22], but do not contain significant information on the more interesting low-wavenumber part of the wave spectrum which contains most of the wave energy.

Fortunately, the scattering measurements, while supporting the Bragg theory, also indicate that it should be regarded only as a first approximation. The Doppler spectra, in particular, exhibit

several features not predicted by the Bragg model. Generally, there is a marked dependence of the anomalies on sea state, suggesting that useful correlations between backscatter signatures and significant sea-state parameters may be discovered by extending the scattering theory to higher order.

Two generalisations have been proposed: the wave-facet interaction model [23, 4, cf. also 3, 9, 10, 20, 21], in which the Bragg-scattering waves are superposed on longer carrier waves, and the higher-order, wave-wave interaction model originally investigated by Rice [18]. The models have been applied hitherto mainly to the cross sections, which show only weak sea-state signatures. In the present paper, we consider their extension to the more strongly sea-state dependent Doppler spectra.

In the cm-dm bands, good agreement with the observed Doppler spectra is obtained with the wave-facet interaction model. The Doppler spectra are found to be quasi-Gaussian and can be characterized to good approximation by the mean frequency and the frequency bandwidth. Both parameters depend on moments of the wave spectrum which are governed by the high-energy, low-wave-number range of the spectrum. They can therefore be used to obtain independent estimates of, say, the mean waveheight and period.

The model allows only for electromagnetic interactions. Basically, the hydrodynamical modulation of short gravity waves by long carrier waves is of considerable interest, not only for the description of the surface wave field, but also for its energy balance. The interactions generally lead to an energy loss of the long waves at a rate which can be estimated from the observed upwind-downwind asymmetry of the cross sections [11]†. However, because of the strong influence of white capping, the interactions cannot yet be described in sufficient detail to be included realistically in computations of the Doppler spectra. Their effect on the Doppler bandwidth is probably negligible, but the mean Doppler frequency may be more strongly modified.

The wave-facet interaction model is valid for electromagnetic wave lengths shorter than about 1 m. Thus it applies in the cm-dm radar band, but not in the dkm band. In the latter case, however, the Bragg theory can be generalised by straightforward extension of the wave-wave interaction analysis to higher order. The relevant

---

†Longuet-Higgins [13] has shown that the momentum loss of short waves breaking on the crests of longer waves results in an energy transfer to the long waves. However, the gain in long-wave kinetic energy due to this process can be shown to be slightly less than the loss of potential energy arising from the simultaneous mass transfer between short and long waves. The net result of both processes is a weak attenuation of the long waves [11].

perturbation parameter of the expansion is given by the ratio of the amplitude of the interacting surface wave to the wave length of the incident radiation. In the first order analysis, the perturbation parameter is proportional to the slope of the scattering Bragg wave, which is small for all electromagnetic wave lengths. At second and higher order, however, the electromagnetic waves interact with longer surface waves of higher amplitude. In this case, the perturbation parameter remains small only if the electromagnetic wave length is large compared with the amplitude of the entire wave field. This condition is satisfied by dkm waves, but not by cm-dm waves.

The requirements for the wave-facet and wave-wave interaction models are found to be mutually exclusive, so that the two expansions cannot be matched in a common region of validity. It is a fortunate coincidence that the theoretical wave length gap corresponds to the gap between the two presently available techniques for measuring electromagnetic backscatter on a synoptic scale.

The second order wave-wave interaction analysis yields a continuous Doppler spectrum superimposed on the first-order Bragg line. The continuum reduces to a particularly simple and useful form when the Bragg wave length is short compared with the wave lengths of the dominant surface waves -- the usual situation for ionospheric modes. In this case, the continuum is identical with the two-sided image of the surface-wave frequency spectrum, centered on the Bragg line as virtual frequency origin. The energy scale of the wave spectrum can be inferred from the observed energy of the Bragg line, independent of transmission or other calibration factors.

Doppler side-band structures observed by Ward [22] and others are not inconsistent with this interpretation. However, most Doppler spectra published hitherto have been analysed from rather short records, so that the continuum is generally not well defined statistically. Longer records are needed to decide whether the one-dimensional frequency spectrum of the surface-wave field can indeed be detected in the Doppler spectrum of backscattered ionospheric modes above the inherent ionospheric noise.

II. THE LOWEST-ORDER SCATTERING MODELS

For electromagnetic waves short compared with the dominant waves of the sea, one might attempt to describe the scattered field by a specular reflexion model, in which the sea surface is represented as an ensemble of locally plane, infinitesimal facets, each of which reflects the incident radiation according to the laws of geometric optics. The cross section σ for the backscattered radiation (the backscattered energy per unit solid angle per unit surface area of the ocean) is then proportional to the number density of facet normals

pointing towards the source. As the distribution of normals in a random surface-wave field is approximately Gaussian, the dependence of log σ on depression angle θ is given by a parabola, with maximum at normal incidence (90° depression angle) and half-width typically of the order 10° (Fig. 1).

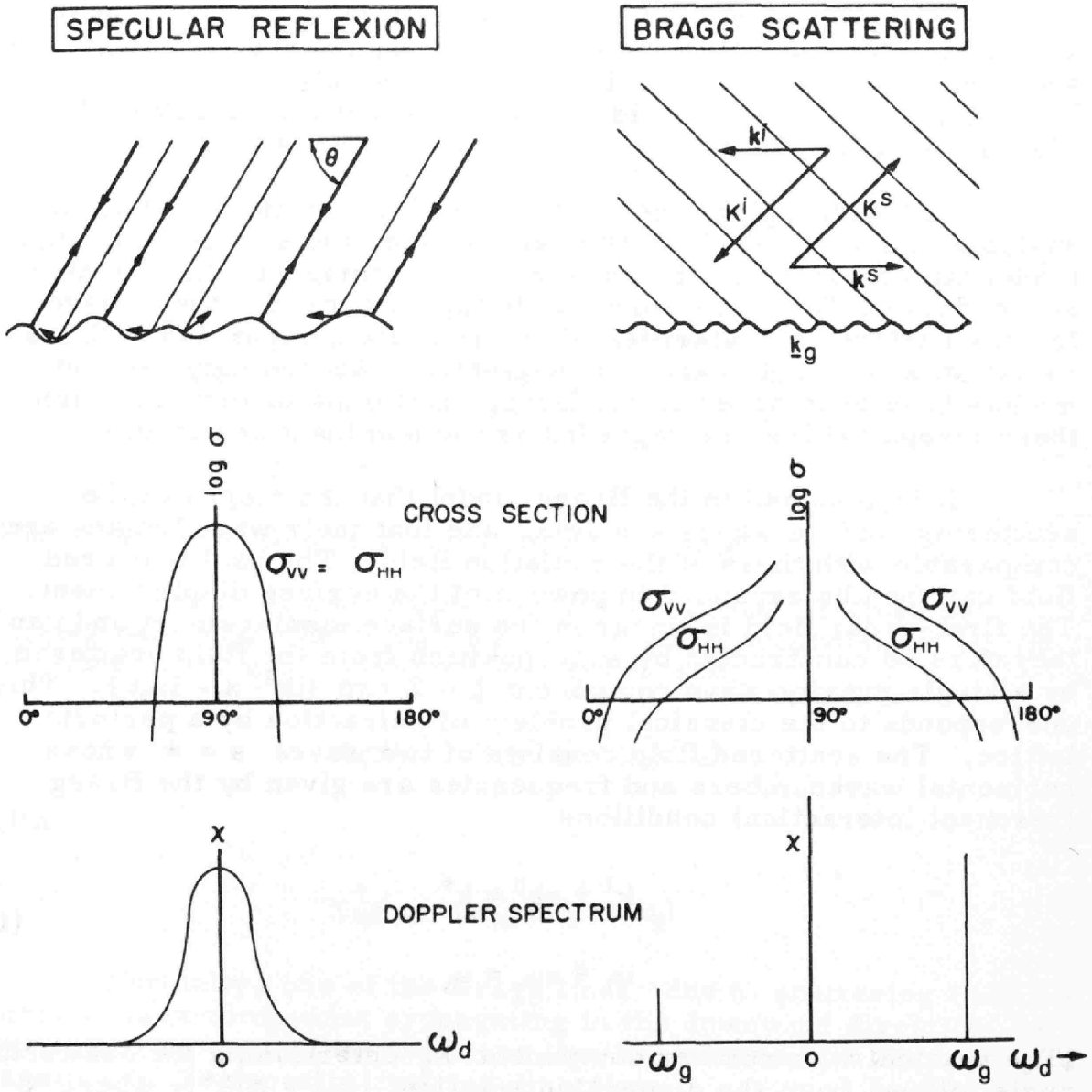

Fig. 1. Cross sections and Doppler spectra according to the specular reflection and first-order Bragg scattering models (qualitative)

The frequencies of the backscattered waves are shifted relative to the frequency of the incident radiation by the Doppler frequency $\omega_f = -2\underset{\sim}{k}^i \cdot \underset{\sim}{u}$ induced by the facet motion, where $\underset{\sim}{K}^i = (\underset{\sim}{k}^i, k_3^i)$ is the wavenumber of the incident radiation and $\underset{\sim}{u}$ the local orbital velocity of the waves. For an approximately linear wave field, $\underset{\sim}{u}$ is a Gaussian variable, and the Doppler spectrum also has a Gaussian shape.

As the backscattered waves are reflected at normal incidence, it follows by symmetry that the cross sections and Doppler spectra are independent of polarisation. Vertical and horizontal polarisation are denoted in Fig. 1 by V and H, respectively, the first index referring to the incident field, the second to the backscattered field. The cross-polarised return VH and HV vanishes.

Although applied successfully by Cox and Munk [5] to the analysis of sun glitter from the sea surface, the specular reflexion model fails to describe the observed electromagnetic backscatter at cm-dm and dkm wave lengths. It appears that for these wave lengths surface irregularities of length scale comparable with the radiation wave length cannot be neglected. Accordingly, recent models have been based on the Bragg scattering theory, in which these irregularities are regarded as the dominant scatterers.

It is assumed in the Bragg model that the slopes of the scattering surface waves are small and that their wave lengths are comparable with those of the radiation field. The backscattered field can then be expanded in powers of the surface displacement. The first-order field is linear in the surface displacement and can therefore be constructed by superposition from the field scattered by a single gravity-wave component $\zeta = Z \exp\{i\underset{\sim}{k}^g \cdot \underset{\sim}{x} - i\omega_g t\}$. This corresponds to the classical problem of refraction by a periodic lattice. The scattered field consists of two waves $s = \pm$ whose horizontal wavenumbers and frequencies are given by the Bragg (resonant interaction) conditions

$$\begin{aligned} \underset{\sim}{k}^i + s\underset{\sim}{k}^g &= \underset{\sim}{k}^s \\ \omega_i + s\omega_g &= \omega_s \end{aligned} \qquad (1)$$

(The vertical wavenumber component k_3^i determining the scattering angle follows from the dispersion relation $|\omega_s| = c|\underset{\sim}{k}^s|$, where c is the velocity of light).

Backscattering ($\underset{\sim}{k}^s = -\underset{\sim}{k}^i$) occurs for the gravity-wave components $\underset{\sim}{k}^g = \pm 2\underset{\sim}{k}^i$. The backscattering cross section is accordingly of the form

$$\sigma_{\alpha\beta} = \sigma^+_{\alpha\beta} + \sigma^-_{\alpha\beta} \qquad (2)$$

where

$$\sigma^s_{\alpha\beta} = T_{\alpha\beta} F_g(-2s\underset{\sim}{k}^i) \quad (\alpha,\beta = V \text{ or } H, \quad s = \pm)$$

and $F_g(\underset{\sim}{k})$ is the surface-wave spectrum, normalised such that the mean square surface displacement $\langle \zeta^2 \rangle = \int F_g(\underset{\sim}{k})\, d\underset{\sim}{k}$. The cornered parentheses denote mean values. (The negative sign of the wave-number in the definition of $\sigma^s_{\alpha\beta}$ has been introduced so that $\sigma^+_{\alpha\beta}$ corresponds to a spectral line with positive Doppler shift, cf. Eq. (3).) $T_{\alpha\beta}$ is a scattering coefficient obtained by expanding the electro-magnetic boundary conditions at the free surface [18]),

$$T_{VV} = \left| \frac{2\omega_i^2}{c^2} \sin^2\theta \, \frac{(1-\epsilon)(\epsilon[1+\cos^2\theta] - \cos^2\theta)}{(\epsilon \sin\theta + \sqrt{\epsilon - \cos^2\theta})^2} \right|^2$$

$$T_{HH} = \left| \frac{2\omega_i^2}{c^2} \sin^2\theta \, \frac{1-\epsilon}{(\sin\theta + \sqrt{\epsilon - \cos^2\theta})^2} \right|^2$$

$$T_{VH} = T_{HV} = 0$$

where ϵ is the dielectric constant of sea water.

The normalized Doppler spectrum $\chi_{\alpha\beta}(\omega_d)$, defined by $\int \chi_{\alpha\beta}(\omega_d)\, d\omega_d = \sigma_{\alpha\beta}$, where $\omega_d = \omega_s - \omega_i$, is given according to (1) by two lines at the gravity-wave frequencies $\pm \omega_g$,

$$\chi_{\alpha\beta}(\omega_d) = \chi^+_{\alpha\beta}(\omega_d) + \chi^-_{\alpha\beta}(\omega_d)$$

with (3)

$$\chi^s_{\alpha\beta}(\omega_d) = \sigma^s_{\alpha\beta}\delta(\omega_d - s\omega_g)$$

Normally, one of the Bragg lines due to scattering from the surface wave component propagating in the downwind direction is very much stronger than the other line associated with the wave propagating in the opposite, upwind direction.

The general properties of the Bragg cross sections and Doppler spectra are indicated qualitatively in the right-hand panels of Fig. 1. In contrast to the specular reflexion model, there is a pronounced dependence on polarisation and appreciable backscatter at small and intermediate depression angles. The cross-polarised return again vanishes.

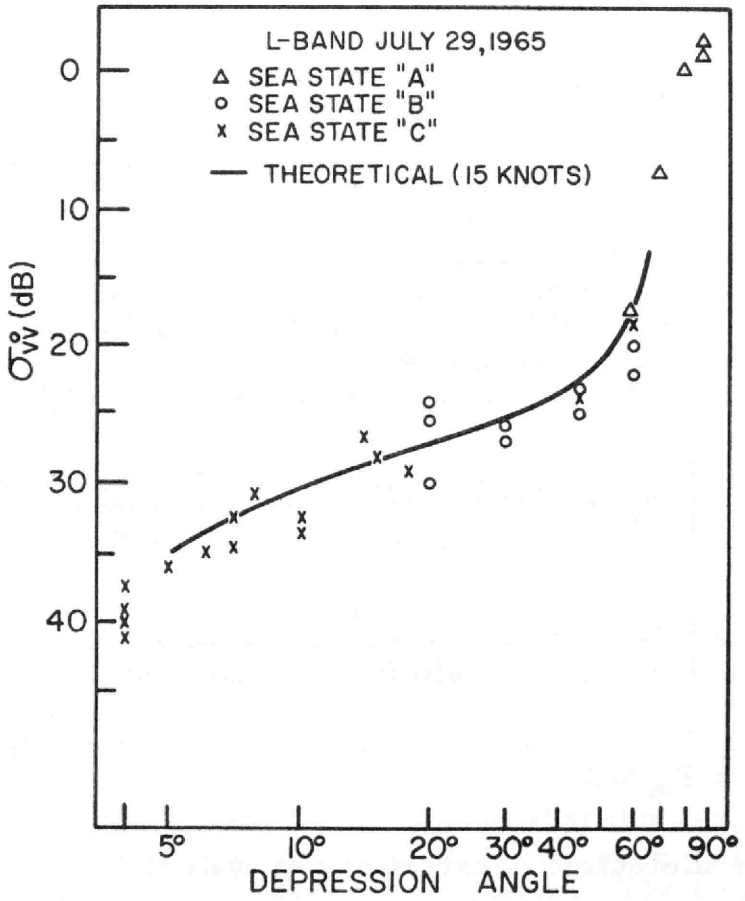

Fig. 2. Theoretical and observed Bragg backscatter cross sections for vertically polarised 24 cm (L band) waves (from Wright [23])

Figure 2 shows a comparison by Wright [23]† of experimental and theoretical Bragg cross sections for vertically polarised cm-dm waves. The surface waves were represented by a Phillips' spectrum $F_g(\underset{\sim}{k}) = (\alpha/2)k^{-4}S(\psi)$, with a uniform half-plane angular spreading function, $S(\psi) = \pi^{-1}$ for $0 \leq |\psi| < \pi/2$, $S(\psi) = 0$ for $-\pi/2 < |\psi| \leq \pi$. The constant α was chosen to fit the observed cross sections, but is not inconsistent with other estimates from direct measurements of gravity-wave spectra (cf. also [15]). Shown in Fig. 3 are theoretical and experimental cross section ratios σ_{VV}/σ_{HH}. The agreement here is also very good, except for the shortest wave length (3.4 cm, 8910 MHz), where scattering by spray may be beginning to mask the

†The theoretical cross sections shown in Figs. 2 and 3 were, in fact, computed for the wave-facet interaction model considered in the next section. However, the deviations from the first-order Bragg model are negligible.

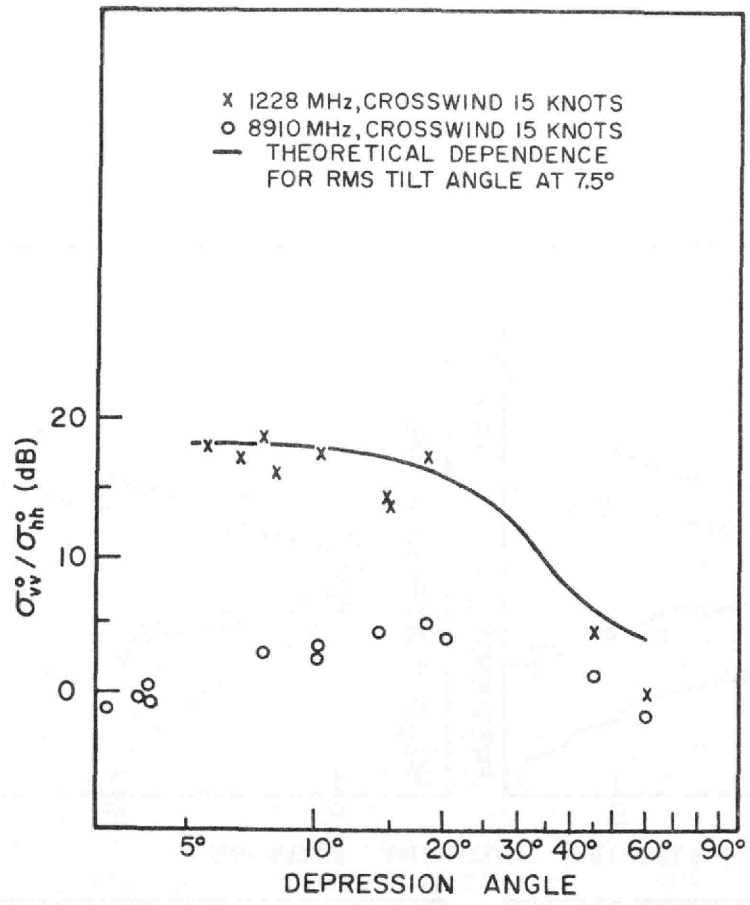

Fig. 3. Theoretical and observed ratios of Bragg backscatter cross sections for vertical and horizontal polarisation at wave lengths 24 cm (1228 MHz) and 3.4 cm (8910 MHz) (from Wright [24])

weak Bragg return for horizontal polarisation. Not predicted by first-order Bragg theory is the observed cross-polarised return, which is generally only slightly smaller than or comparable with the backscatter for horizontal polarisation; this can be explained by the wave-facet interaction model [23].

Although the observed cross sections σ_{VV} and σ_{HH} are in good agreement with theory, the Doppler spectra for these polarisations point to limitations of the first-order model. In the cm-dm bands, the Bragg lines are found to be broadened into Gaussian shaped distributions with bandwidths of the same order as the Bragg frequency (cf. Fig. 4., from Valenzuela and Laing [20]). Earlier measurements by Hicks et al. [13] indicate that the mean frequencies of the distributions -- which were not measured by Valenzuela and Laing -- may also be considerably higher, by factors of the order 2 to 4, than the theoretical Bragg frequency.

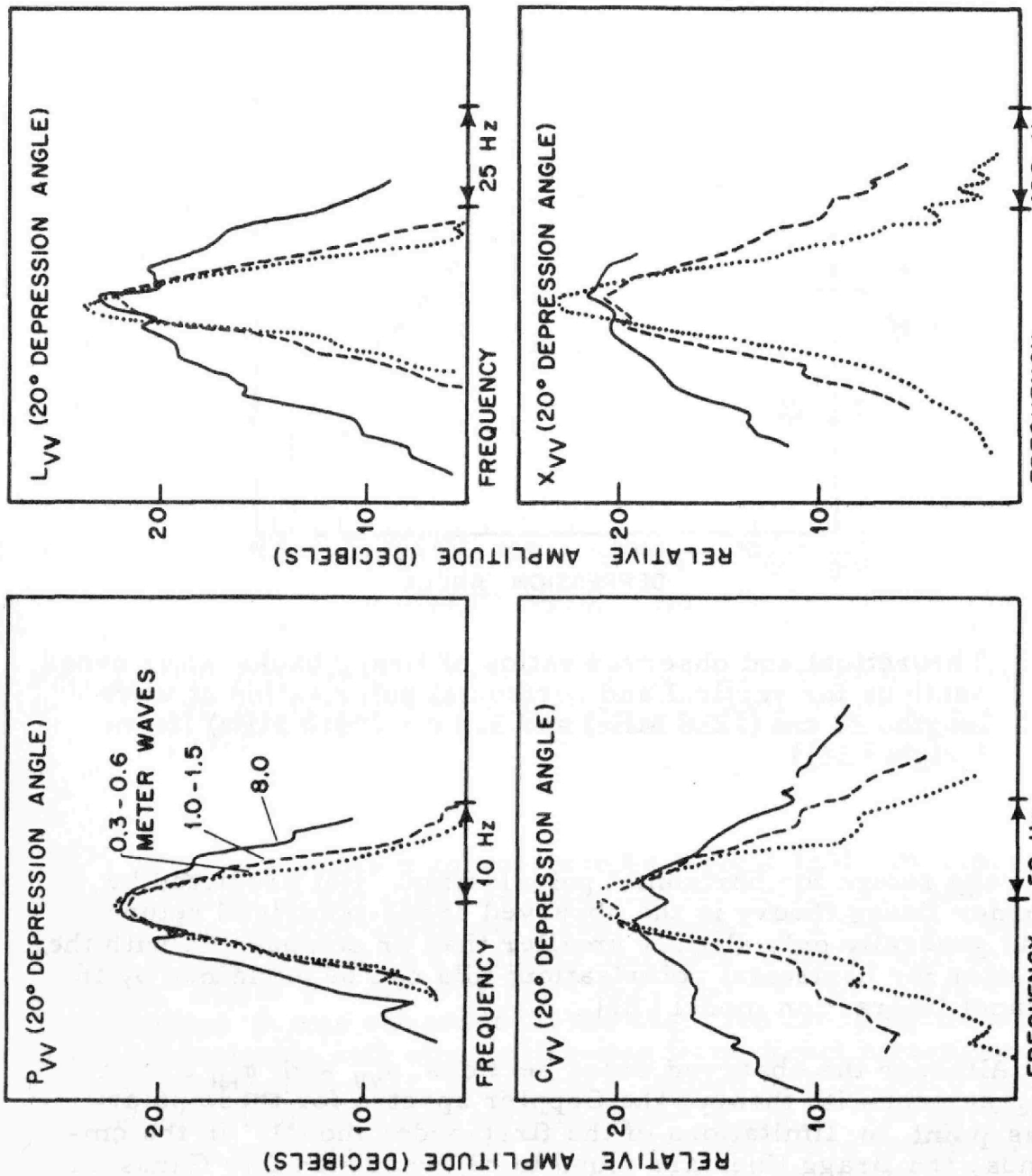

Fig. 4. Examples of vertically polarised Doppler backscatter spectra in bands P (70 cm), L (24 cm), C (6.7 cm) and X (3.4 cm). (From Valenzuela and Laing [20]).

In the decameter bands, the observed broadening and shift of the Bragg lines are much weaker. Instead, the Doppler spectra show pronounced side band structures (cf. Fig. 11, from Ward [22], and similar spectra in Crombie [6] and elsewhere). The basic difference in structure of the Doppler spectra observed in the cm-dm and dkm bands lends support to theoretical considerations calling for alternative expansion procedures in the two wave length ranges.

III. THE WAVE-FACET INTERACTION MODEL

In order to treat the scattering waves as small perturbations of a plane surface, it is assumed in the Bragg theory that the wave amplitudes are small compared with the wave length of the incident radiation. In a strict sense, the expansion is valid if this condition is satisfied not only for the Bragg waves, but for the entire surface displacement. Thus the theory is not rigorously applicable to short electromagnetic waves of a few cm wave length, although the long surface waves of high amplitude which violate the expansion condition do not enter in the final scattering expressions. Various workers [e.g. 3, 4, 10, 20, 21, 23] have suggested that this formal shortcoming may be remedied by dividing the surface-wave spectrum into two parts, a high-wavenumber scattering region, and the energy-containing region at low wavenumbers which defines the "sea." The "sea" is then treated as a random carrier wave which modulates the scattering by the superimposed Bragg waves. If the Bragg wave length π/k^i is short compared with a typical wave length $2\pi/k^c$ of the sea, the carrier wave may be represented locally as a plane facet, and the first-order scattering theory applied in the reference frame of the moving facet.

The model involves additional conditions besides the two-scale assumption that it is possible to define a facet diameter D intermediate between the carrier and scattering wave length scales,

$$(k^i)^{-1} \ll D \ll (k^c)^{-1} \tag{4}$$

The finite facet size implies an indeterminacy $\Delta k = O(1/D)$ of the scattering wavenumber, which corresponds to an angular spread $\Delta\theta = O\{(K^i D \sin\theta)^{-1}\}$ of the backscattered beam. The wave-facet interaction model is meaningful only if $\Delta\theta$ is small compared with the change in effective depression angle introduced by the facet slope $\partial\zeta/\partial x = O(k^c\zeta)$, where ζ is the carrier-wave amplitude. This requires $k^c\zeta DK^i \sin\theta \gg 1$, or, since $Dk^c \ll 1$, on account of [4],

$$K^i\zeta \sin\theta = k_3^i\zeta \ggg 1 \tag{5}$$

Similarly, a wavenumber broadening Δk corresponds to a frequency broadening of the Bragg line of order $\Delta\omega = (d\omega_g/dk^g)\,\Delta k = (\omega_g/2k^g) \cdot \Delta k$ (ignoring capillary effects). The model assumes that this is small compared with the Doppler shift $\omega_f = -2\underset{\sim}{K}^i \cdot \underset{\sim}{u}$ induced by the facet velocity $\underset{\sim}{u}$. For $u = O(\omega_c \zeta)$, where ω_c is a typical carrier-wave frequency, this requires

$$DK^i \omega_c \zeta k^i/\omega_i = DK^i (k^i k^c)^{1/2} \zeta >> 1$$

Substituting $Dk^c << 1$, this is equivalent to

$$K^i \zeta (k^i/k^c)^{1/2} >>> 1 \tag{6}$$

Since $k^i/k^c >> 1$, the frequency condition (6) is less critical than the corresponding condition (5) for the angular resolution. The inequality (5) is normally fairly well satisfied at conventional radar wave lengths for surface-wave heights of order 1 m and higher (except for small depression angles, where the model breaks down, in any case because of shadowing effects). For electromagnetic wave lengths longer than about 1 m the inequality (5) is normally no longer valid, even though the two-scale inequality (4) may still apply.

The total backscattered energy is obtained in the wave-facet interaction model by summing over the contributions from all scattering facets. Introducing a facet probability distribution $p(\underset{\sim}{\lambda})$ with respect to the five basic facet parameters $\underset{\sim}{\lambda} = (\lambda_1, \lambda_2, \lambda_3, \lambda_4, \lambda_5)$, where

$$(\lambda_1, \lambda_2, \lambda_3) = (u_1, u_2, u_3) = \text{facet velocity (= local long-wave orbital velocity)},$$

and $(\lambda_4, \lambda_5) = (\partial\zeta/\partial x_1, \partial\zeta/\partial x_2) \equiv (n_1, n_2) =$ facet slope, the Doppler spectrum is given by

$$\chi^s_{\alpha\beta} = \int [\tilde{\sigma}^s_{\alpha\beta} \delta(\omega_d - s\tilde{\omega}_g - \omega_f)]\; p(\underset{\sim}{\lambda})\; d\underset{\sim}{\lambda} \tag{7}$$

where $\tilde{\sigma}^s_{\alpha\beta}$, $\tilde{\omega}_g$ represent, respectively, the Bragg cross section and gravity-wave frequency in the facet reference frame.

To the modulated Doppler spectrum (7) of the first-order Bragg field should be added the modulated spectrum of the zero'th order field reflected from a plane facet, as described by the specular reflexion model. However, this is important only near vertical incidence and will be ignored in the following.

Experimentally, the probability distribution $p(\underset{\sim}{\lambda})$ is found to be approximately Gaussian, in accordance with the theoretical distri-

bution for a random, linear gravity-wave field,

$$p(\underset{\sim}{\lambda}) = (2\pi)^{-5/2} |C|^{-1/2} \exp\left\{-\frac{1}{2} C_{ij}^{-1} \lambda_i \lambda_j\right\} \tag{8}$$

The covariance matrix C_{ij} can be evaluated from the surface-wave spectrum and the linear wave solutions,

$$C_{ij} = \left[\begin{array}{cc:ccc} g\overline{k_1^2/k} & g\overline{k_1k_2/k} & & O & \\ g\overline{k_1k_2/k} & g\overline{k_2^2/k} & & & \\ \hdashline & & g\overline{k} & -\overline{\omega k_1} & -\overline{\omega k_2} \\ O & & -\overline{\omega k_1} & \overline{k_1^2} & \overline{k_1k_2} \\ & & -\overline{\omega k_2} & \overline{k_1k_2} & \overline{k_2^2} \end{array}\right] \tag{9}$$

where $\overline{k_\alpha k_\beta/k} = \int F_g(\underset{\sim}{k})(k_\alpha k_\beta/k)\, d\underset{\sim}{k}$, etc.

We note that the facet Doppler shift ω_f is correlated not only with the facet velocity, but through the correlation $\langle u_3 n_i \rangle$ also with the facet slope,

$$\langle \omega_f n_i \rangle = -2k_3^i \langle u_3 n_i \rangle \tag{10}$$

For small wave slopes, the factor in square parentheses in Eq. (7) can be expanded in powers of n_i. The integration can then be carried out explicitly for each term of the expansion yielding a solution of the form

$$\chi_{\alpha\beta}(\omega_d) = \chi^{+}_{\alpha\beta}(\omega_d) + \chi^{-}_{\alpha\beta}(\omega_d)$$

with

$$\chi^{s}_{\alpha\beta}(\omega_d) = (\tilde{\sigma}^{s}_{\alpha\beta})_0 \frac{\exp\left\{-(\omega_d - s\omega_g)^2/2\langle\omega_f^2\rangle\right\}}{(2\pi\langle\omega_f^2\rangle)^{1/2}} \left[1 + q_1^s + q_2^s + \ldots\right] \tag{11}$$

where q_1^s, q_2^s, ... are polynomials in $(\omega_d - s\omega_g)$ of order 1, 2, ... in the facet slope,

$$q_1^s = \frac{\langle \omega_f n_i \rangle (\omega_d - s\omega_g)}{\langle \omega_f^2 \rangle} \left\{ \left(\frac{\partial}{\partial n_i} \tilde{\sigma}^{s}_{\alpha\beta}\right)_0 / (\tilde{\sigma}_{\alpha\beta})_0 + \frac{s(\omega_d - s\omega_g)}{\langle \omega_f^2 \rangle} \left(\frac{\partial \tilde{\omega}_g}{\partial n_i}\right)_0 \right\} \tag{12}$$

$$q_2^s = \left\{ \langle n_i n_j \rangle + \frac{\langle \omega_f n_i \rangle \langle \omega_f n_j \rangle}{\langle \omega_f^2 \rangle^2} \left[(\omega_d - s\omega_g)^2 - \langle \omega_f^2 \rangle \right] \right\} \cdot$$

$$\cdot \left\{ \frac{1}{2} \left(\frac{\partial^2 \tilde{\sigma}^s_{\alpha\beta}}{\partial n_i \partial n_j} \right)_0 / \tilde{\sigma}^s_{\alpha\beta})_0 + s \frac{(\omega_d - s\omega_g)}{\langle \omega_f^2 \rangle} \left[\frac{1}{2} \left(\frac{\partial^2 \tilde{\omega}_g}{\partial n_i \partial n_j} \right)_0 + \left(\frac{\partial \tilde{\omega}_g}{\partial n_i} \frac{\partial \tilde{\sigma}^s_{\alpha\beta}}{\partial n_j} / \tilde{\sigma}^s_{\alpha\beta} \right)_0 \right] \right.$$

$$\left. + \frac{(\omega_d - s\omega_g)^2 - \langle \omega_f^2 \rangle}{2\langle \omega_f^2 \rangle^2} \left(\frac{\partial \tilde{\omega}_g}{\partial n_i} \frac{\partial \tilde{\omega}_g}{\partial n_j} \right)_0 \right\} \tag{13}$$

The subscript 0 refers to values at $\underset{\sim}{n} = 0$.

To lowest order, the Doppler spectra for vertical and horizontal polarisation are identical Gaussian distributions with mean frequency $\langle \omega \rangle = s\omega_g$ and variance

$$\langle (\omega - \langle \omega \rangle)^2 \rangle = \langle \omega_f^2 \rangle = 2 \left\{ k^i_\ell k_m \langle u_\ell u_m \rangle + (k^i_3)^2 \langle u_3^2 \rangle \right\} \tag{14}$$

$$(\ell, m = 1, 2)$$

The distribution represents an ensemble of Bragg lines of equal energies displaced by their appropriate facet Doppler frequencies ω_f.

The higher-order corrections q_1^2, q_2^2, ... represent distortions of the Gaussian distribution due to the variations in energy of the Bragg lines associated with variations in the carrier-wave slope. These affect the shape of the Doppler spectrum through the correlation between facet slopes and facet Doppler frequency, Eq. (10). The degree of distortion depends on the depression angle and polarisation. In the cross-polarised case, the zero'th and first-order terms disappear, since $(\tilde{T}_{VH})_0 = (\partial/\partial n_i \; \tilde{T}_{VH})_0 = 0$, so that the Doppler spectrum is non-Gaussian already to lowest order.

Computations of the Doppler spectrum were made for a Pierson-Moskowitz [16] spectrum using a half-plane cosine-to-the-fourth spreading factor,

$$F_g(\underset{\sim}{k}) = \begin{cases} \frac{4\alpha}{3\pi} k_1^{-4} \exp \{ -\beta(\omega_0/\omega)^4 \} & \text{for} \quad k_1 > 0 \\ 0 & \text{for} \quad k_1 < 0 \end{cases}$$

with $\alpha = 0.0081$, $\beta = 0.74$ and $\omega_0 = g/U$, where U is the wind velocity, assumed parallel to the x_1 axis. The same spreading factor was taken for both scattering and carrier waves.

For a Pierson-Moskowitz spectrum, $\langle \omega_f^2 \rangle \sim U^2$ and $\langle \omega_f n_i \rangle \sim U$. The slope moments $\langle n_i n_j \rangle$ diverge logarithmically at high wavenumbers. To obtain finite $\langle n_i n_j \rangle$, the "carrier-wave" spectrum was cut off at an upper wavenumber $k_g/10$. The exact position of the cut-off is not critical for the evaluation of $\langle n_i n_j \rangle$, and the slope moments themselves enter only rather weakly in the second-order term q_2^s of the expansion (11). However, the existence of a divergence as such points to a conceptual difficulty of the wave-facet interaction model. It appears that for an asymptotic k^{-4} spectrum the carrier-wave region of the spectrum cannot be rigorously separated from the Bragg-scattering region.

Figure 5 shows the computed half-power bandwidths for the lowest-order Gaussian spectrum as a function of wave height. The values compare well with measurements by Valenzuela and Laing [20].

Deviations from the Gaussian form due to the higher-order corrections q_1^s and q_2^s are represented in Figs. 6 - 9 in terms of the mean frequency $\langle \omega \rangle / \omega_g$ and the frequency bandwidth $\langle (\omega - \langle \omega \rangle)^2 \rangle / \langle \omega_f^2 \rangle$, normalised by their appropriate values for the zero'th order Gaussian spectrum.

The strongest correction is found for the mean frequency, particularly for horizontal polarisation. The dependence on depression-angle and polarisation, shown in Fig. 6 for $U = 20$ m/s, is found to be very similar at all wind speeds. The absolute values of the frequency shifts increase approximately linearly with wind speed, Fig. 7. Qualitatively, the polarisation and wind-speed dependence of the mean Doppler frequency are in agreement with measurements made by Hicks et al. [13] at low depression angles of about 5°. However, the theory is not strictly applicable in this case on account of shadowing effects.

The bandwidth corrections (Figs. 8 and 9) remain rather small for depression angles less than 45° and limited azimuth angles ψ relative to the wind. Larger deviations in the cross-wind directions depend strongly on the spreading factors, which are rather uncertain for these angles. The experimental dependence of the Doppler bandwidth on radar frequency and polarisation [20] tends to be somewhat larger and have a different trend than the corrections shown in Figs. 8 and 9. Valenzuela and Laing [20] suggest that these effects may be due partly to spray. To a fair approximation, the observed bandwidths can be represented for small and intermediate angles ψ and θ by the zero'th order Gaussian bandwidth.

Both the bandwidth and mean frequency vary significantly with wave height and can therefore be used for estimates of sea state. For the one-parametrical family of spectra considered in the present example, the two estimates are not independent. However, in general the mean square bandwidth $\langle (\omega - \langle \omega \rangle)^2 \rangle \approx \langle \omega_f^2 \rangle$ (Eq. 14) and the mean

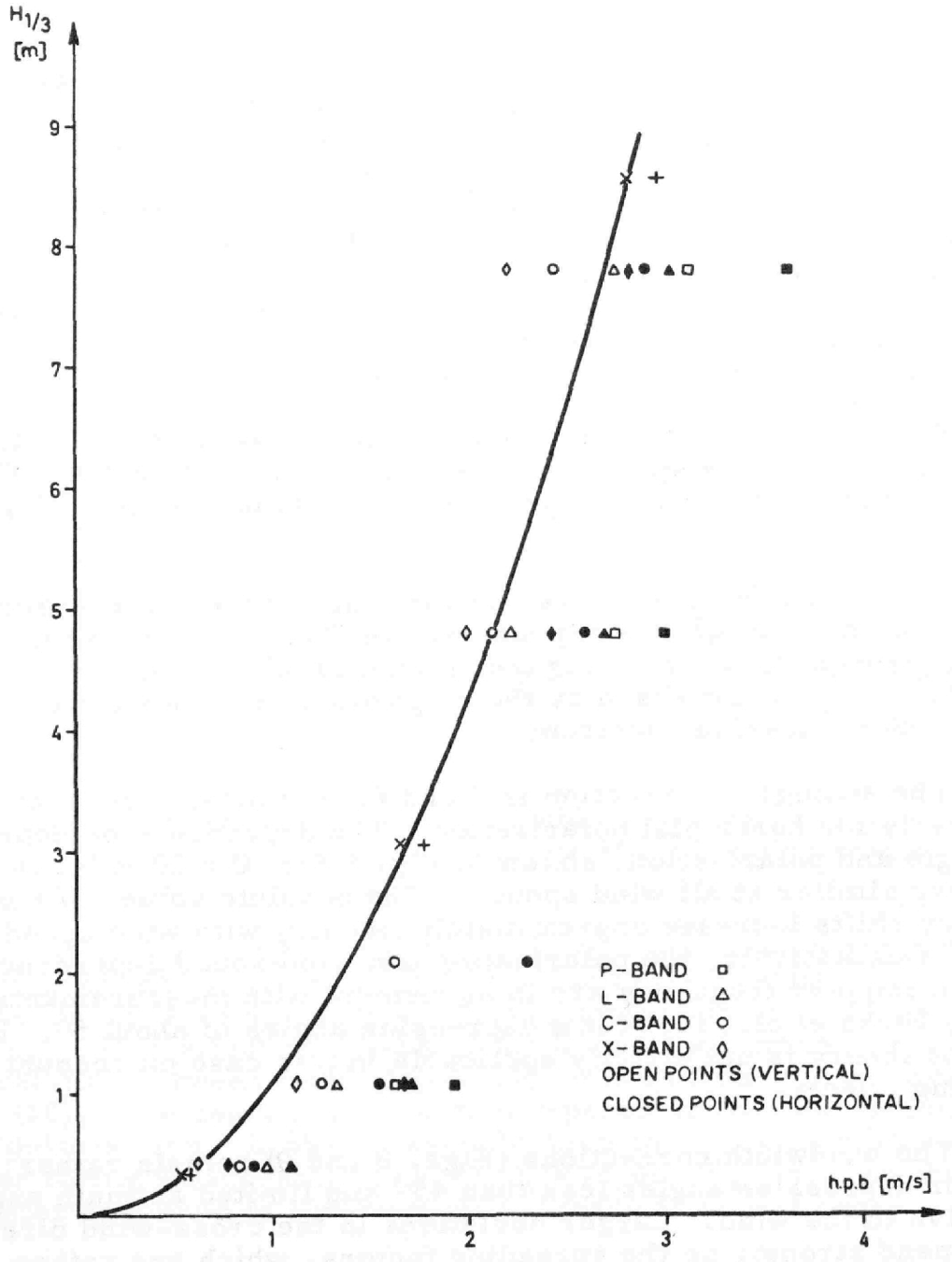

Fig. 5. Comparison of theoretical half-power bandwidths (h.p.b.) for zero'th order Gaussian spectrum with measurements by Valenzuela and Lang [20]. Doppler frequencies are in units of equivalent velocities $U_d = \omega_d/2k$. Theoretically, a Pierson-Moskowitz spectrum with $\cos^4\psi$ spreading function yields

$$\text{h.p.b.}\,[\text{m/s}] = 1.06\left\{\frac{\cos^2\theta}{6}\,(4\cos^2\psi + 1) + \sin^2\theta\right\}^{1/2} (H_{1/3}[\,\text{m}\,])^{1/2}$$

where the significant wave height $H_{1/3} \approx 4\langle\zeta^2\rangle^{1/2} = 0.209\ U^2/g$. The computations were made for $\psi = 0^\circ$, $\theta = 20^\circ$.

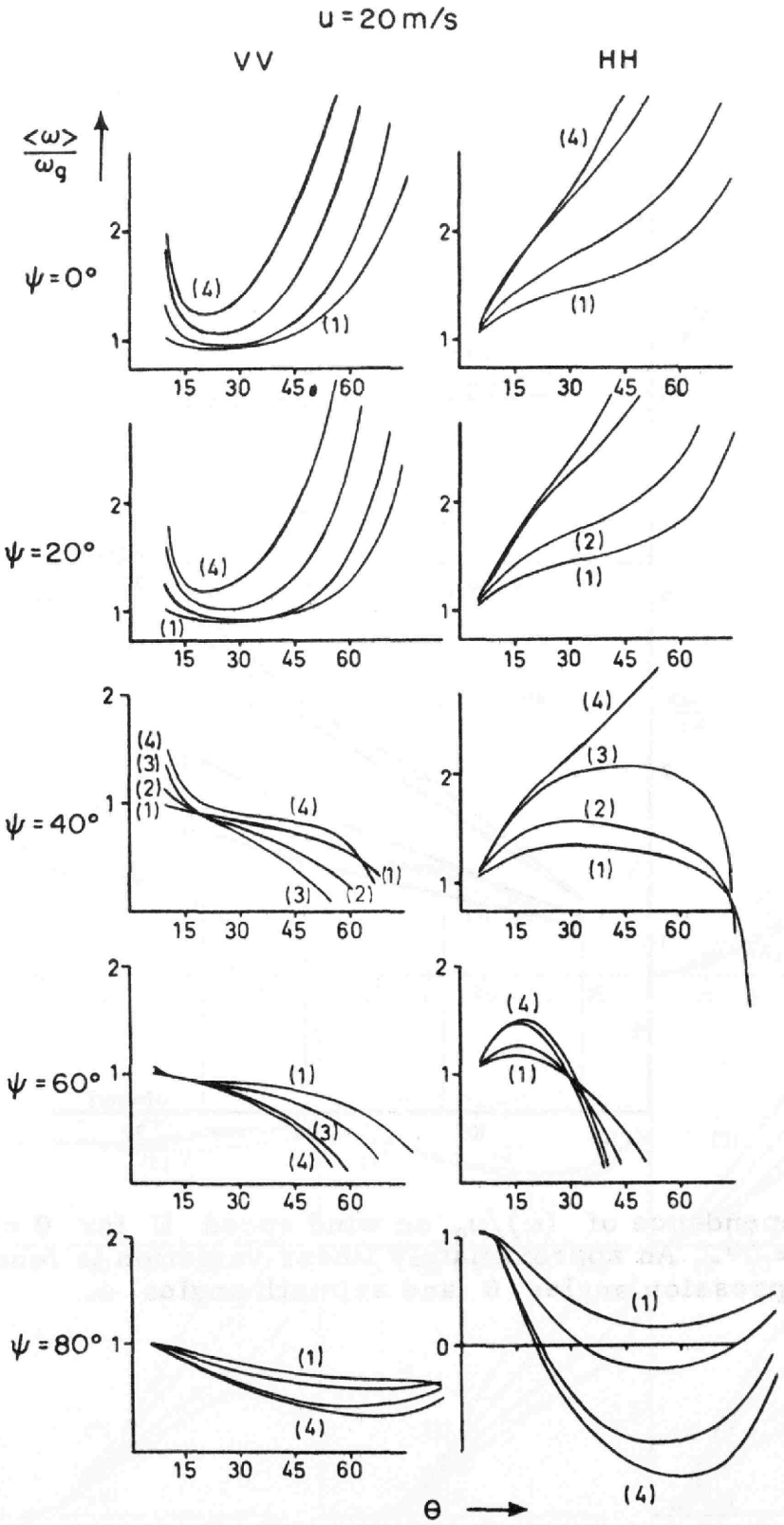

Fig. 6. Ratios of mean Doppler frequency $\langle\omega\rangle$ to Bragg frequency ω_g for the wave-facet interaction model at windspeed U = 20 m/s. The indices 1, 2, 3, 4 refer to P, L, C and X bands, respectively. The computations include terms up to order q_2^s in the expansion (11). To this approximation, the cross polarised case yields $\langle\omega\rangle = \omega_g$.

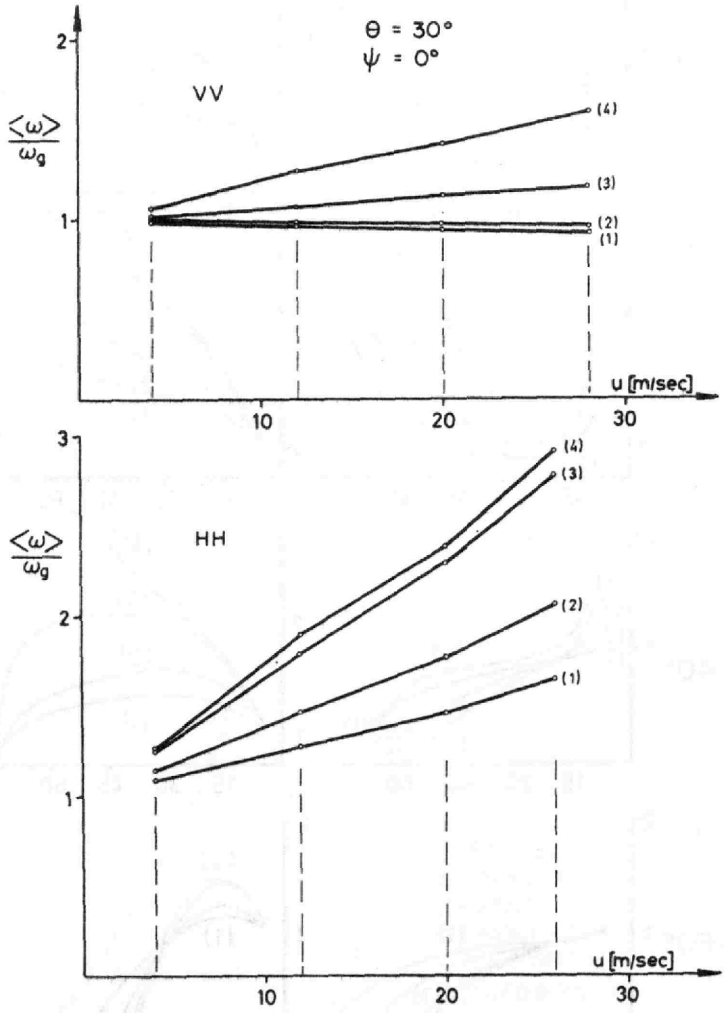

Fig. 7. Dependence of $\langle\omega\rangle/\omega_g$ on wind speed U for $\theta = 30^o$, $\psi = 0^o$. An approximately linear variation is found for all depression angles θ and azimuth angles ψ.

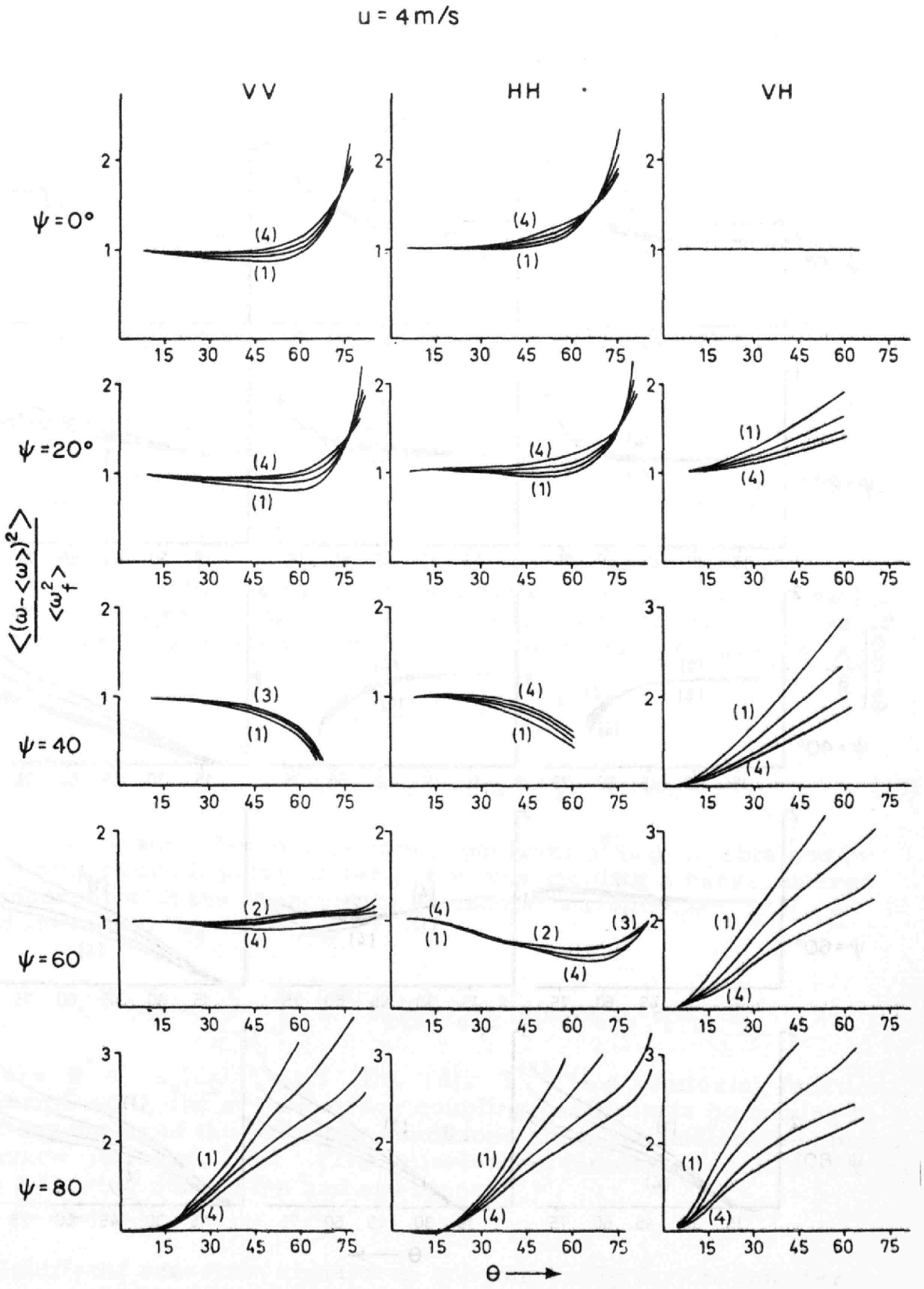

Fig. 8. Frequency variance of the Doppler spectrum computed to order q_2^s, normalised by the variance $\langle\omega_f^2\rangle$ of the zero'th order Gaussian distribution (U = 4 m/s).

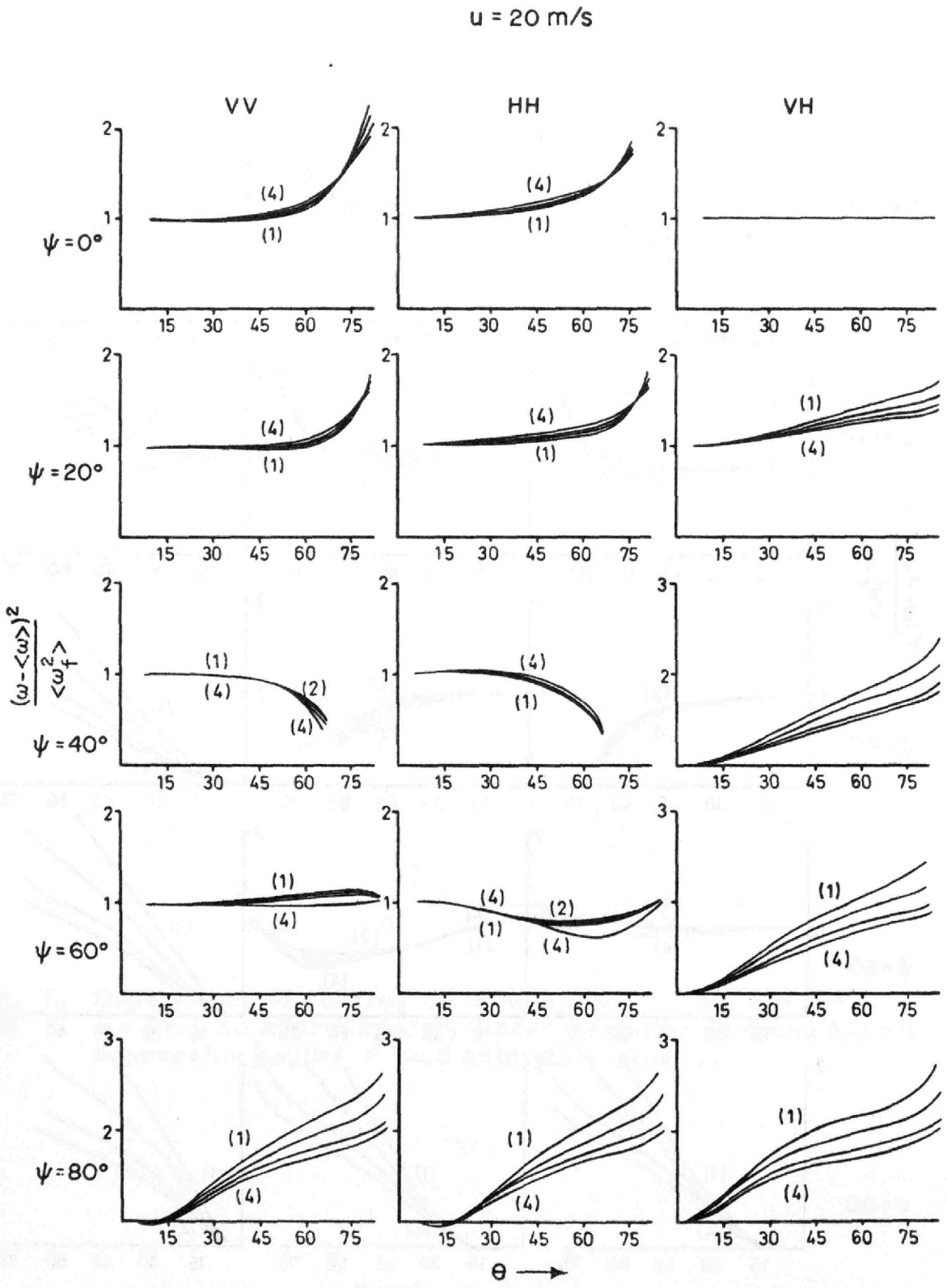

Fig. 9. Same as Fig. 8 with wind speed U = 20 m/s

product $\langle \omega_f n_i \rangle$ (Eq. 10), which is responsible for most of the mean-frequency variation, depend on differently weighted moments of the gravity-wave spectrum. The two Doppler parameters can therefore be used to obtain independent estimates of two sea-state parameters --for example, the mean wave height and mean wave period.†

IV. HIGHER-ORDER WAVE-WAVE INTERACTIONS

For HF waves longer than about 10 m, the Bragg model can be generalised by straightforward extension of the wave-wave interaction expansion to higher order. In this case, the perturbation parameter $k_3^i \zeta$ is normally a small quantity even when ζ is defined as the surface displacement of the complete wave field, and there is no need to consider the long waves of high amplitude separately. In fact, the wave-facet interaction model is not applicable for HF waves on account of the angular resolution condition (5). The inequality $k_3^i \zeta \ll 1$ and condition (5) are mutually exclusive, representing a wave length gap between the wave-facet and higher-order wave-wave interaction models extending from a few fractions of a meter to about 10 meters.

At second order, the wave-wave interaction analysis yields scattered waves through interactions with pairs of gravity-wave components a, b satisfying the next-order Bragg conditions

$$\underset{\sim}{k}^i + \sigma_a \underset{\sim}{k}^a + \sigma_b \underset{\sim}{k}^b = \underset{\sim}{k}^s$$

$$\omega_i + \sigma_a \omega_a + \sigma_b \omega_b = \omega_s \qquad (\sigma_a, \sigma_b = \pm) \tag{15}$$

The second-order Doppler spectrum $\chi^{(2)}(\omega_d)$ is obtained by summing over all pairs of surface waves yielding a backscattered component with the appropriate horizontal wavenumber $\underset{\sim}{k}^s = -\underset{\sim}{k}^i$ and frequency $\omega_s = \omega_i + \omega_d$,

$$\chi^{(2)}(\omega_d) = \sum_{\sigma_a, \sigma_b} \int T^{(2)} F_g(\underset{\sim}{k}^a) F_g(\underset{\sim}{k}^b) \delta(\omega_d - \sigma_a \omega_a - \sigma_b \omega_b) \, d\underset{\sim}{k}^a \tag{16}$$

where $\underset{\sim}{k}^b = -\sigma_b(2\underset{\sim}{k}^i + \sigma_a \underset{\sim}{k}^a)$ (Eq. 15). $T^{(2)}$ is a scattering function determined by the second-order coupling coefficients occurring in the expansion of the boundary conditions about the undisturbed plane surface (cf. Ref. (18)). (The polarisation indices are irrelevant for the following discussion and are ignored.)

---

† Significant sea-state signatures are found only for the Doppler spectra and not the cross sections. On integrating Eq. (11) with respect to frequency the dependence on the moments $\langle \omega_f^2 \rangle$ and $\langle \omega_f n_i \rangle$ disappears, leaving only a weak sea-state dependence through the slope moments $\langle n_i n_j \rangle$.

The scattering function $T^{(2)}$ includes both electromagnetic and hydrodynamic interactions at the free surface. For wave lengths in the HF range and longer, the hydrodynamic interactions can probably be described to fair approximation by classical hydrodynamical theory, independent of the effects of wave breaking. Equation (16) represents the random-field expression of nonlinear effects such as nonsinusoidal wave forms†, nonlinear phase velocities, etc., that have been variously suggested as explanation of the observed side bands of HF Doppler spectra.

In the limit of an incident wave short compared with the principal waves of the sea, the dominant interactions at finite depression angles are electromagnetic. The largest contributions to the integral in (16) arise in this case from interactions in which one of the gravity-wave components, say $\underset{\sim}{k}^a$, lies near to the peak of the spectrum. Since $k^a \ll k^i$, the second component k^b is then approximately equal to the Bragg component, $\sigma_b \underset{\sim}{k}^b \approx -2\underset{\sim}{k}^i$ (cf. Eq. (15) and Fig. 10). The side condition $\omega_d = \sigma_a\omega_a + \sigma_b\omega_b = \text{const}$ (expressed by the δ-function in the integral) defines an integration curve in the $\underset{\sim}{k}^a$ plane which is given approximately by the circle $k^a = \text{const}$. This follows by noting that, on account of Eq. (15), the variation δk^a corresponds to an equally large variation $\pm \delta k^b$. But for $k^a \ll k^b$, the associated frequency variation $\delta\omega_b$ is generally small compared with the variation $\delta\omega_a$, since $d\omega_b/dk^b \ll d\omega_a/dk^a$. Hence the side condition $\omega_d = \text{const}$ reduces to $\omega_a = \text{const}$. It is shown below that, at finite depression angles, $T^{(2)}$ is independent of $\underset{\sim}{k}^a$ for $k^a \ll k^b$, and the integration over the directions of $\underset{\sim}{k}^a$ for fixed k^a can then be readily carried out, yielding

$$\chi^{(2)}(\omega_d) = \chi^{(2)+}(\omega_d) + \chi^{(2)-}(\omega_d)$$

where (17)

$$\chi^{(2)s}(\omega_d) = 2T^{(2)} F_g(-s2\underset{\sim}{k}^i)\,[E_g(\omega_d - s\omega_g) + E_g(s\omega_g - \omega_d)]$$

and $E_g(\omega)$ is the one-dimensional frequency spectrum of the wave field, with $\langle \zeta^2 \rangle = \int_0^\infty E_g(\omega)\, d\omega$. (The factor 2 arises through interchange of the components a and b in Fig. 10.)

Thus each Bragg line appears as the carrier of a second-order, two-sided image of the surface-wave frequency spectrum. Physically, the Doppler continuum arises, as in the case of the wave-facet interaction model, through the modulation of the first-order

---

† These include the often invoked "higher interference orders" occurring in the Bragg scattering by a lattice. They are generated only if the periodic scattering field is not a purely sinusoidal disturbance but contains higher harmonics.

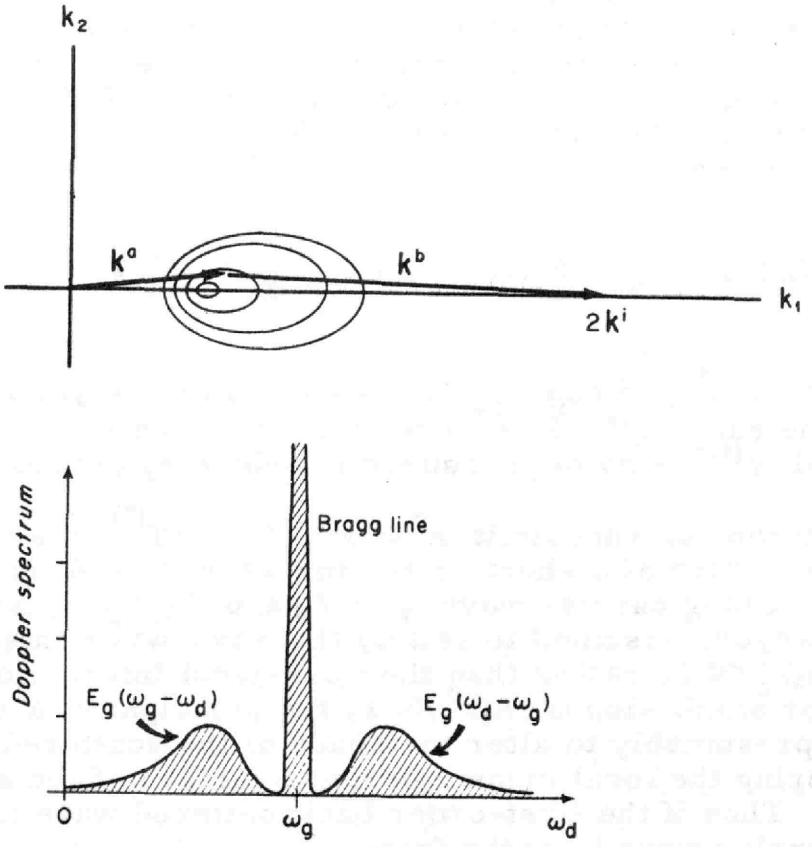

Fig. 10. Upper panel. Interacting gravity-wavenumbers $\underset{\sim}{k}^a$, $\underset{\sim}{k}^b$ for a spectral-peak wavenumber small compared with the Bragg wavenumber $2k^i$. Strong contributions to the second-order Doppler spectrum $\chi^{(2)}(\omega_d)$ arise when $\underset{\sim}{k}^a$ is close to the spectral peak. Contour lines indicate curves of constant spectral energy.
Lower panel. The associated second-order Doppler spectrum $\chi^{(2)}$ consists of two images of the wave frequency spectrum E_g reflected on either side of the Bragg line.

Bragg field by long surface waves of high amplitude. However, in the present case the Doppler shift is not determined by the frequency shift $\omega_f = -2\,\underset{\sim}{k}^i \underset{\sim}{u}$ induced by the long-wave orbital velocities, but rather by the intrinsic long-wave frequencies ω_a. Each low-frequency component splits the first-order Bragg line $\omega_s^{(1)} = \omega_i + \sigma_b\omega_b$ into two lines $\omega_s^{(2)} = \omega_s^{(1)} \pm \omega_a$. Since $u \approx \zeta\omega_a$, the regions of validity for the wave-facet and wave-wave interaction models may also be expressed, respectively, as $\omega_a << \omega_f$ and $\omega_a >> \omega_f$.

A useful feature of the relation (17) is that it defines the surface-wave spectrum in absolute energy units independent of electromagnetic calibration factors, which are difficult to establish for long-range ionospheric mode propagation. Using Eqs. (3) and (2) to eliminate the surface-wave spectrum at the Bragg wavenumber, Eq. (17) becomes

$$E_g(\omega_d - s\omega_g) + E_g(s\omega_g - \omega_d) = \frac{T^{(1)}}{2T^{(2)}} \frac{\chi^{(2)s}(\omega_d)}{\epsilon^{(1)s}} \qquad (s = \pm) \tag{18}$$

where $\epsilon^{(1)s} = \int \chi^{(1)s}(\omega_d)\, d\omega_d$ is the energy of the first-order Bragg line. The ratio $T^{(1)}/2T^{(2)}$ can be determined from theory, and $\chi^{(2)s}$ and $\epsilon^{(1)s}$ may be measured in arbitrary energy units.

In the relevant limit $k^a \ll k^b$, $T^{(1)}/2T^{(2)}$ may be deduced from the picture of a short scattering wave $\zeta_b = A_b \exp\{i(\underset{\sim}{k}^b \underset{\sim}{x} - \omega_b t)\}$ riding on a long carrier wave $\zeta_a = A_a \exp\{i(\underset{\sim}{k}^a \underset{\sim}{x} - \omega_a t)\}$ (which is now, however, assumed to satisfy the wave-wave interaction condition $A_a k_3^i \ll 1$, rather than the wave-facet interaction condition (5)). For small slopes $A_a k^a \ll 1$, the principal effect of the carrier wave is presumably to alter the phase of the scattered field by raising and lowering the local mean reference surface of the short scattering waves†. Thus if the first-order backscattered wave in the absence of the carrier wave is of the form

$$\varphi^{(1)} = C^{(1)} A_b A_i \exp\{i(\underset{\sim}{k}^i + \sigma_b \underset{\sim}{k}^b)\underset{\sim}{x} - i(\omega_i + \sigma_b \omega_b)t + ik_3^s x_3\}$$

where A_i is the amplitude of the incident field, $C^{(1)}$ is a first-order coupling coefficient, and $\underset{\sim}{k}^i + \sigma_b \underset{\sim}{k}^b \approx -\underset{\sim}{k}^i$, $k_3^s \approx -k_3^i$, the modulated scattered wave in the presence of the carrier wave will be given approximately by

$$\tilde{\varphi} = e^{2ik_3^i \zeta_b} \varphi^{(1)} \approx (1 + 2ik_3^i \zeta_b)\varphi^{(1)} \equiv \varphi^{(1)} + \varphi^{(2)} \tag{19}$$

Thus

$$\varphi^{(2)} = C^{(2)} A_a A_b A_i \exp\{-i\,\underset{\sim}{k}^i \underset{\sim}{x} - i(\omega_i + \omega_d)t - ik_3^i x_3\} \tag{20}$$

with $C^{(2)} = 2ik_3^i C^{(1)}$. Expressed in terms of a continuous energy spectrum, this is readily found to correspond to a scattering function ratio

---

†A more detailed investigation indicates that slope effects can be ignored if $k^a \ll k_3^i = k^i \sin\theta$.

$$\frac{T^{(2)}}{T^{(1)}} = \frac{1}{4}\left|\frac{C^{(2)}}{C^{(1)}}\right|^2 = (k_3^i)^2 \qquad (21)$$

For small depression angles ($k_3^i \ll k^i$), the effect of the carrier-wave slope becomes comparable with the phase shift induced by the vertical displacement, and the relations (20), (21) should be modified to include additional terms dependent on k^a. However, this requires a more detailed investigation of the electromagnetic and hydrodynamic interactions.†

Examples of Doppler spectra obtained by Ward [22] from the sea echo of 21.840 MHz (14 m) waves at ranges near 3000 km are shown in Fig. 11. The analysis was based on short records of one minute duration, so that the continuum is poorly resolved statistically and individual spectra vary strongly. However, there is some indication of two side-band structures appearing on either side of a central Bragg peak. Theoretically, the Bragg line should lie at 0.48 Hz, which agrees well with the central peak of the first spectrum shown, but is somewhat to the left of the main peaks in the other cases. The displacement of the side lobes relative to the Bragg peak is of the order 0.1 Hz expected for typical ocean-wave frequencies.

The ratio of the side-band energy $\epsilon^{(2)} = \int \chi^{(2)}(\omega_d)\, d\omega_d$ to the energy $\epsilon^{(1)}$ of the Bragg line is given according to Eqs. (18) and (21) by

$$\epsilon^{(2)}/\epsilon^{(1)} = 4(k_s^i)^2 \langle \zeta^2 \rangle$$

Ward estimates a depression angle of 12°, which yields

$$\epsilon^{(2)}/\epsilon^{(1)} = 0.036 \langle (\zeta\,[\mathrm{m}])^2 \rangle$$

The observed ratios of order unity correspond to root mean square wave heights of about 5 m, which appear rather high, but not impossible.

More plausible estimates of the wave height may have resulted from a more accurate determination of the scattering function ratio $T^{(2)}/T^{(1)}$ at small depression angles. Contamination of the observed spectra by ionospheric Doppler shifts may be an alternative explanation of the high ratios $\epsilon^{(2)}/\epsilon^{(1)}$. A spurious interaction between the Bragg line and the low frequency ionospheric Doppler spectrum could also have been introduced in the present experiment by the data analysis, since the Doppler spectra appear to have been computed -- as is often done -- from the time series of

† Note added in proof: A detailed analysis has recently been carried out by D. E. Barrick "Dependence of Second-Order Doppler Side Bands in HF Sea Echo on Sea State," to appear in 1971 G-AP Internat. Symp. Digest.

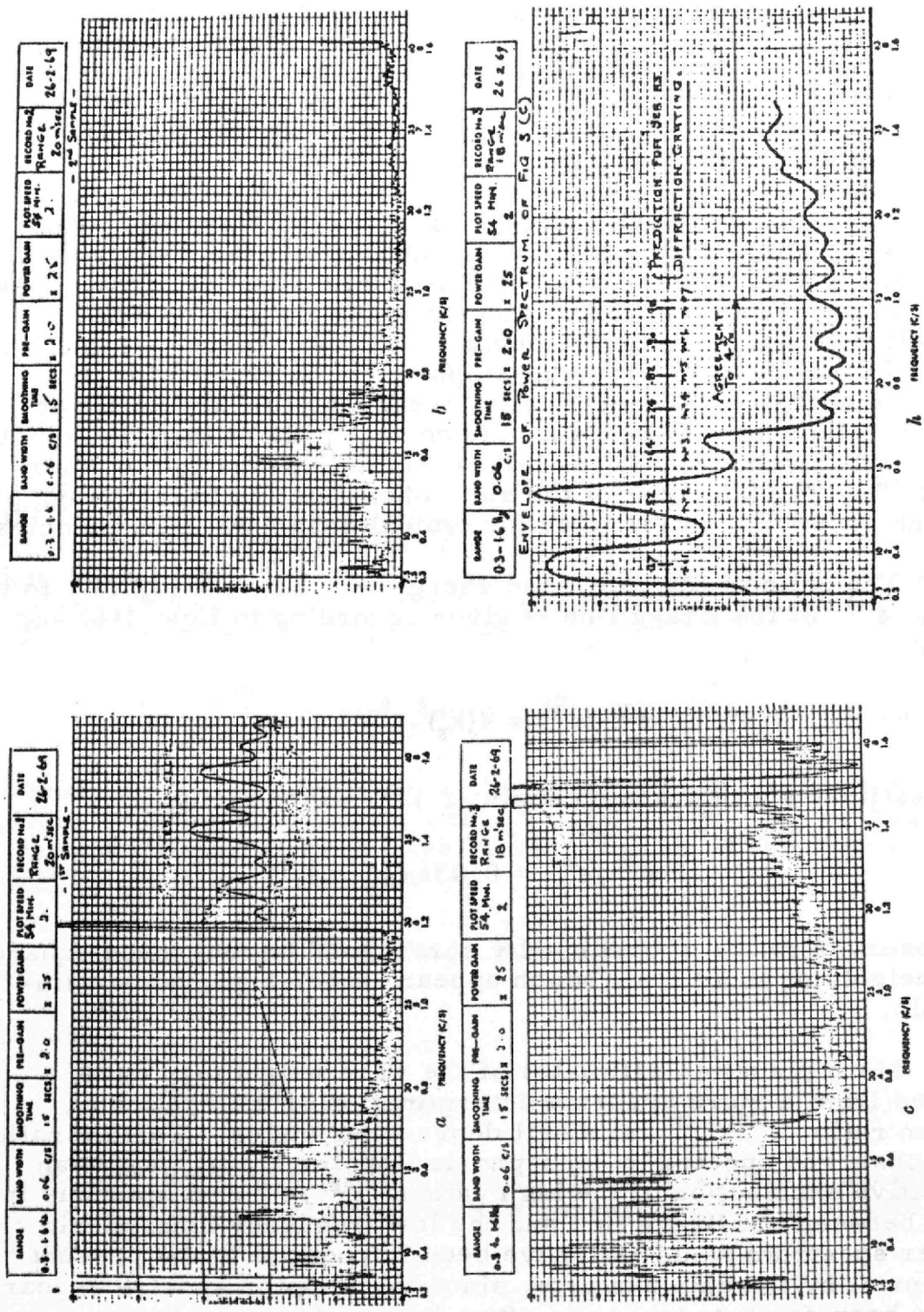

Fig. 11. Doppler spectra of 21.84 MHz (14 m) sea echo at ranges of 2700 km (18 ms) and 3000 km (20 ms), from Ward [22].

the signal phase (or phase cosine), which is nonlinearly related to the complex signal amplitude. More detailed investigations using longer time series are needed to decide whether the ocean wave spectrum can be extracted from the Doppler spectrum of long range HF sea echo in the presence of unavoidable ionospheric noise.

ACKNOWLEDGMENT

This work was supported in part by the Office of Naval Research under Contract No. ONR N00014-69-C-0057.

REFERENCES

1. Barnett, T. P., "Generation, dissipation and prediction of wind waves," J. Geophys. Res., 73, 513-534, 1968.

2. Barnett, T. P., Holland, C. H. Jr. and Yager, P., "General technique for wind-wave prediction with application to the S. China Sea," Westinghouse Res. Lab. Rep., June, 1969.

3. Barrick, D. E. and Peake, W. H., "A review of scattering from surfaces with different roughness scales," Radio Sci., 3, 865-868, 1968.

4. Bass, F. G., Fuks, I. M., Kalmykov, A. I., Ostrovsky, I. E., and Rosenberg, A. D., "Very high frequency radiowave scattering by a disturbed sea surface," IEEE Trans., AP-16, 554-568, 1968.

5. Cox, C. M. and Munk, W. H., "Measurement of the roughness of the sea surface from photographs of the sun's glitter," J. Opt. Soc. Am., 44, 838-850, 1954.

6. Crombie, D. P., "Doppler spectrum of sea echo at 13.56 mc/s," Nature, 175, 681-682, 1955.

7. Daley, J. C., Ransone, J. T. Jr., Burkett, J. A. and Duncan, J. R., "Sea-clutter measurements on four frequencies," Nav. Res. Lab. Rep. 6806, 1968.

8. Daley, J. C., Ransone, J. T. Jr., Burkett, J. A. and Duncan, J. R., "Upwind-downwind-crosswind sea-clutter measurements," Nav. Res. Lab. Rep. 6881, 1969.

9. Ewing, G. C., ed., Oceanography from Space, Woods Hole Oceanogr. Inst., Ref. No. 65-10, 1965.

10. Guinard, N. W. and Daley, J. C., "An experimental study of a sea clutter model," Proc. IEEE, 58, 543-550, 1970.

11. Hasselmann, K., "On the mass and momentum transfer between short gravity waves and larger-scale motions," J. Fluid Mech., 50, 189, 1971.

12. Hasselmann, K., "Determination of ocean wave spectra from Doppler radio return from the sea surface," Nature, 229, 16-17, 1971.

13. Hicks, B. L., Knable, N., Kavaly, J. J., Newell, G. S., Ruina, J. P. and Sherwin, C. W., "The spectrum of X-band radiation backscattered from the sea surface," J. Geophys. Res., 65, 825-837, 1960.

14. Longuet-Higgins, M. S., "A nonlinear mechanism for the generation of sea waves," Proc. Roy. Soc. A. 311, 371-389, 1969.

15. Munk, W. H. and Nierenberg, W. A., "High frequency radar sea return and the Phillips saturation constant," Nature, 224, 1285, 1969.

16. Pierson, W. J. and Moskowitz, L., "A proposed spectral form for fully developed wind seas based on the similarity theory of S. A. Kitaigorodskii," J. Geophys. Res., 69, 5181-5190, 1964.

17. Pierson, W. J., Tick, L. J. and Baer, L., "Computer based procedure for preparing global wave forecasts and w nd field analysis capable of using wave data obtained by a space craft," 6th Naval Hydrodynamic Symposium, Washington, Office of Naval Res., Washington, D. C., 1966.

18. Rice, S. O., "Reflection of electromagnetic waves from slightly rough surfaces," Comm. Pure Appl. Math., 4, 351-378, 1951.

19. Semenov, B., "An approximate calculation of scattering on the perturbed sea surface," IVUZ Radiofizika (USSR), 9, 876-887, 1966.

20. Valenzuela, G. R. and Laing, M. B., "Study of Doppler spectra of radar sea echo," J. Geophys. Res., 75, 551-563, 1970.

21. Valenzuela, G. R., Laing, M. B. and Daley, J. C., "Ocean spectra for the high frequency waves from airborne radar measurements," 1970 (subm. to J. Mar. Res.).

22. Ward, J. F., "Power spectra from ocean movements measured remotely by ionospheric radar backscatter," Nature, 223, 1325-1330, 1969.

23. Wright, J. W., "A new model for sea clutter," IEEE Trans. AP-16, 217-223, 1968.